



Research article

Compositional stability in medium and high-entropy alloys of CoCrFeMnNi system under ion irradiation



Q. Xu ^{a,*}, H.Q. Guan ^b, S.S. Huang ^b, Z.H. Zhong ^c, H. Watanabe ^d, M. Tokitani ^e

^a Institute for Integrated Radiation and Nuclear Science, Kyoto University, Osaka 590-0494, Japan

^b Key Laboratory of Materials Modification by Laser, Ion and Electron Beams (Dalian University of Technology), Ministry of Education, Dalian 116024, China

^c School of Materials Science and Engineering, Hefei University of Technology, Hefei 230031, China

^d School Research Institute for Applied Mechanics, Kyushu University, Fukuoka 816-8580, Japan

^e National Institute for Fusion Science, Gifu 509-5292, Japan

ARTICLE INFO

Article history:

Received 16 May 2022

Received in revised form 15 July 2022

Accepted 5 August 2022

Available online 9 August 2022

Keywords:

Medium-entropy alloy

High-entropy alloy

Ion irradiation

Segregation

Calculation

ABSTRACT

The equiatomic high-entropy alloy (HEA) CoCrFeMnNi not only has excellent mechanical properties but also good irradiation resistance. However, the mechanical properties of some equiatomic medium-entropy alloys (MEAs) are superior to those of CoCrFeMnNi HEA. In this study, the irradiation resistance and changes in composition due to irradiation in CoCrNi and CoCrFeNi MEAs and CoCrFeMnNi HEA are investigated. Thin film samples of the MEAs and HEA and Ni used for comparison were irradiated with up to 1.7×10^{19} ions/m² of 2.4 MeV Cu ions at 673 and 873 K. The average damage in the observed area was 1 displacement per atom (dpa). No voids were observed in any of the MEA and HEA samples even after irradiation at 873 K; however, large voids were formed in Ni irradiated at 873 K. This indicates that the irradiation resistance of CoCrNi and CoCrFeNi MEAs and CoCrFeMnNi HEA was better than that of Ni. In addition, the formation of stacking fault tetrahedra (SFTs), a type of vacancy cluster, at 873 K was much more pronounced in CoCrNi and CoCrFeNi MEAs than in CoCrFeMnNi HEA. Therefore, the irradiation resistance of CoCrNi and CoCrFeNi MEAs is lower than that of CoCrFeMnNi HEA. Moreover, significant Cr segregation occurred in the CoCrNi and CoCrFeNi MEA samples irradiated at 873 K. In contrast, no segregation occurred in CoCrFeMnNi HEA. First-principles calculation results show that the formation rate of Cr-dumbbells is higher in CoCrNi and CoCrFeNi MEAs than in CoCrFeMnNi HEA, and that Cr interstitials are more stable in the MEAs. Therefore, Cr segregation is more likely to occur in the MEAs. Element segregation may affect the irradiation resistance of the alloys.

© 2022 Elsevier B.V. All rights reserved.

1. Introduction

High-entropy alloys (HEA) are usually alloys that contain five or more elements in equal proportions. A typical HEA with excellent strength and toughness is CoCrFeMnNi, which has been widely studied [1–6]. CoCrFeMnNi HEA also has good irradiation resistance [7–11]. Medium-entropy alloys (MEA) are composed of three or four elements in equal proportions, similar to a HEA. Three- (CoCrNi) and four-element MEAs from the CoCrFeNi system are single-phase solid solutions with a face-centered cubic (FCC) structure similar to that of CoCrFeMnNi HEA. CoCrNi and CoCrFeNi MEAs have similar mechanical properties to CoCrFeMnNi HEA [12,13]. However, fewer studies have been performed on the irradiation resistance of CoCrNi and CoCrFeNi MEAs compared to that of CoCrFeMnNi HEA. The

limited research results available show that the irradiation resistance of CoCrNi MEA is worse than that of CoCrFeMnNi HEA [14]. The cause of the decreased irradiation resistance is not well understood.

In general, irradiation with high-energy particles produces the same numbers of interstitial and vacancy defects. The defects produced by high-energy ions and neutrons are spatially non-uniform because of cascade damage. Moreover, because the migration energy of interstitials in metals is lower than that of vacancies, interstitials can migrate at faster rates. In thin film samples, the escape of interstitials from the surface of the sample, leaves behind many vacancies. Cascade generation during high-energy particle irradiation and vacancy cluster formation under supersaturated vacancy states have therefore been investigated in film samples with thicknesses of several tens of nanometers to about 100 nm [15–17]. In addition, because the migration of vacancies often leads to the diffusion of solute atoms in alloys, the presence of excess vacancies may promote element segregation and precipitate formation.

* Corresponding author.

E-mail address: xu.qiu.8z@kyoto-u.ac.jp (Q. Xu).

In the present study, thin-film samples of CoCrNi and CoCrFeNi MEAs and CoCrFeMnNi HEA were irradiated by heavy ions, and the damage to their microstructures and compositional stability investigated. The differences between the irradiation resistance mechanisms of CoCrNi and CoCrFeNi MEAs and CoCrFeMnNi HEA are discussed.

2. Experimental procedure

2.1. Sample preparation and ion irradiation

Similar to CoCrFeMnNi HEA fabrication [8], CoCrNi and CoCrFeNi MEAs were fabricated in a vacuum induction furnace. The purity of each element was higher than 99.9 wt%. These HEA and MEAs were homogenized in vacuum at 1473 K for 10 h and 12 h, respectively. Approximately 1 mm-thick plates were cut from the HEA and MEA ingots and rolled to 0.1 mm. Transmission electron microscopy (TEM) samples with a diameter of 3 mm were punched from the 0.1 mm-thick sheets. The TEM samples were electropolished in a HClO_4 (25%) and CH_3COOH (75%) solution at 15 V to remove the oxide film on their surface, following by annealing in vacuum at 1273 K for 1 h to eliminate processing defects. Thin-film TEM samples of the HEA and MEAs were electropolished in HClO_4 (5%) and CH_3COOH (95%) solutions at 60 V. In addition, pure Ni (99.999%) was also used in this study for comparison with the HEA and MEAs, which was annealed at 973 K for 2 h. The Ni thin-film sample was prepared in the same manner as the HEA and MEA samples.

The HEA, MEA, and Ni thin-film samples were irradiated by 2.4 MeV Cu ion at the high temperatures of 673 K and 873 K using a Tandem type accelerator (model 4110 made by High Voltage Engineering Europe (HVEE)) installed at the Research Institute for Applied Mechanics, Kyushu University [18]. Each thin film sample was placed in the heating holder of a TEM installed in front of the accelerator target chamber and irradiated with an ion fluence of up to $1.6 \times 10^{19} / \text{m}^2$ under a vacuum of $1 \times 10^{-5} \text{ Pa}$ or higher. Fig. 1 shows the damage and Cu deposition in CoCrFeMnNi HEA and CoCrNi and CoCrFeNi MEAs irradiated with up to $1.6 \times 10^{19} \text{ Cu/m}^2$ of 2.4-MeV Cu ions simulated using the SRIM code under the ion distribution and quick calculation damage mode [19]. The threshold displacement energy of each element in the HEA and MEAs was estimated to be 40 eV with reference to the steels [20]. The densities of the CoCrNi and CoCrFeNi MEAs and CoCrFeMnNi HEA were 8.332, 8.215, and 8.059 g/cm³, respectively. For comparison, Fig. 1 also shows the

calculation results for Ni that was subjected to the same irradiation as the HEA and MEAs. To easily compare the damage caused by ion irradiation in the HEA, MEAs, and Ni, where the ion irradiation fluence was the same, the threshold displacement energy of Ni was estimated to be 40 eV [21] instead of the usually used value of 24 eV [22]. As shown in Fig. 1, there was no significant difference in the damage distribution and Cu deposition caused by Cu ion irradiation in the HEA, MEAs, and Ni. The damage peak was located 600 nm from the surface of the sample and the amount of damage was two displacements per atom (dpa), whereas the Cu-ion peak was 800 nm from the surface. The average damage in the TEM observation range (approximately 200 nm) was approximately 1 dpa, and the Cu ions were hardly stopped at this thickness.

2.2. Defect observation and composition analysis

TEM observations were carried out along the [011] direction with an operating diffraction of $g=200$. The thickness of the observation area was estimated using an equal-thickness contour that satisfied the Bragg reflection condition. The extinction distance of a material, ξ_g , depends on the electron wavelength and the atomic scattering factor of the material and can be calculated as [23]:

$$\xi_g = \frac{\pi V \cos \theta}{\lambda f(\theta)} \quad (1)$$

where V is the volume of the unit cell, θ the Bragg angle, λ the wavelength of the electron beam, and $f(\theta)$ the atomic scattering amplitude of the material. The atomic scattering amplitudes of the main elements are summarized in Ref. [24]. The extinction distance ξ_g during the observation of the CoCrNi and CoCrFeNi MEAs and CoCrFeMnNi HEA along the [011] direction with an operating diffraction of $g=200$ using a 200 keV electron beam was thus approximately 37.4 nm regardless of the number of elements in the alloys. For reference, the extinction distance ξ_g of Ni was 34.9 nm under the same observation conditions. Interstitial-type dislocation loop formation was observed in a slightly thick (approximately 130 nm) region at which there were no excess vacancies except near the surface. In contrast, the formation of defect clusters other than interstitial-type dislocation loops were observed in a thin region (approximately 60 nm) where vacancies dominated. In addition, the compositional changes of the ion-irradiated CoCrNi and CoCrFeNi MEAs and CoCrFeMnNi HEA were investigated through mapping measurements performed using an energy-dispersive X-ray spectroscopy (EDS) system attached to a scanning transmission electron microscope (STEM).

2.3. First-principles calculation method

Interactions between interstitials with the same and different elements were investigated using first-principles calculations. The calculation method was described in detail in [25] and briefly summarized here. All the calculations were based on density functional theory (DFT) and performed using the Vienna ab-initio simulation package (VASP) [26,27]. The exchange-correlation function was described using the generalized gradient approximation (GGA) parameterized by Perdew, Burke, and Emzerhof (PBE) [28]. The total energy and force convergence criteria were 0.1 meV and 20 meV/Å, respectively. The cutoff energy of the plane wave for CoCrFeNi MEA and CoCrFeMnNi HEA was taken as 400 eV, while that for CoCrNi MEA was taken as 300 eV. The calculations were performed under constant-volume conditions, and each atom was relaxed. A $3 \times 3 \times 3$ supercell with a total of 108 atoms and a $3 \times 3 \times 5$ supercell with a total of 180 atoms were used for the CoCrNi and CoCrFeNi MEA calculations and the CoCrFeMnNi HEA calculations, respectively. The atomic arrangement in the equiatomic MEA and HEA alloys was optimized in the manner employed in our previous study [25]. The

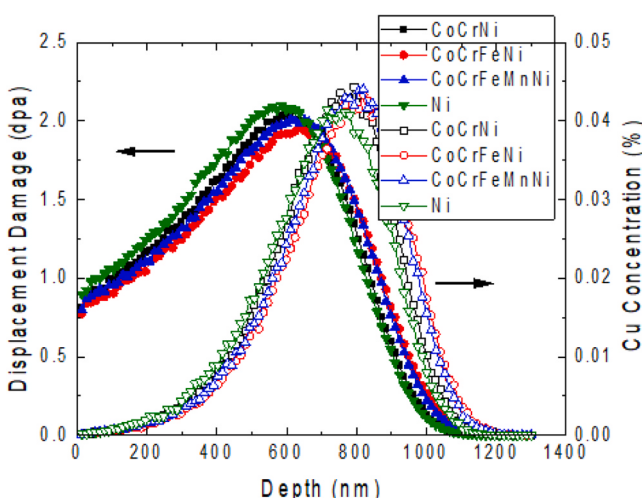


Fig. 1. Depth distribution of displacement damage and Cu ions induced by irradiation with up to $1.6 \times 10^{19} \text{ ions/m}^2$ of 2.4 MeV Cu ions in CoCrNi and CoCrFeNi MEAs, CoCrFeMnNi HEA, and Ni calculated using the SRIM computer code.

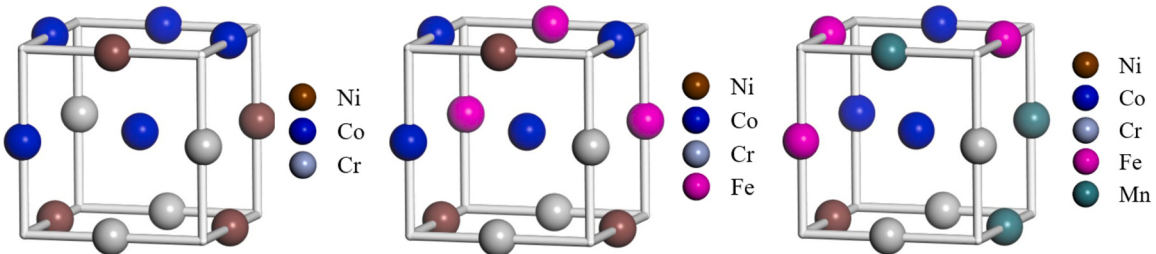


Fig. 2. Unit cell with optimized elemental arrangement in CoCrNi (left figure) and CoCrFeNi (middle figure) MEAs, and CoCrFeMnNi HEA (right figure).

structures were modelled using the similar atomic environment (SAE) approach [29]. In this approach, a similar local atomic environment is established for all the lattice sites in the solid solution. This method differs from the special quasi-random structure (SQS) method, in which the atomic correlation functions are mimicked to approach a fully random solid solution [30]. We randomly selected an environment with a relatively uniform distribution as the unit cell. The proportions of the various elements within the unit cell were therefore approximately equal, and there was little difference between units with different configurations. Fig. 2 shows a unit cell with the optimized elemental arrangement in the CoCrNi (left figure) and CoCrFeNi (middle figure) MEAs and CoCrFeMnNi HEA (right figure).

The self-interstitial defect formation energy, E_f^f , was calculated based on the difference between the energy of the defect lattice (E_{N+1} for interstitials) and that of the reference state, E_N , where N refers to the number of reference-state atoms. E_f^f is given by:

$$E_f^f = E_{N+1} - (E_N - \mu_p) \quad (2)$$

where μ is the chemical potential of the atom and p the type of atom (Co, Cr, Fe, Mn, Ni) [23].

3. Results and discussion

3.1. Damaged microstructure induced by ion irradiation at low temperature of 673 K

Fig. 3 shows bright-field images of the microstructures in the CoCrNi MEA, CoCrFeNi MEA, and CoCrFeMnNi HEA thin films after

ion irradiation at 673 K. For comparison, the microstructures induced by irradiation in Ni are also shown in the same figure. As described in Section 2, the amount of damage in the observed region was 1 dpa. The average thickness of the observation area was 130 nm. In irradiated Ni, black loop-like defects marked by red arrows in the figure were formed (in color figure). These defects are interstitial-type dislocation loops. In addition, black dot-like defects marked by blue arrows (in color figure), which were much smaller than the dislocation loops, were also formed. In contrast, no dislocation loops with clear shapes like those in Ni were formed in the CoCrNi and CoCrFeNi MEAs and CoCrFeMnNi HEA, but high densities of black dot-like defects were formed after irradiation. There were two types of black dot-like defects comprising large and small defects similar to those in Ni. The densities of defects induced by irradiation in the CoCrNi and CoCrFeNi MEAs, CoCrFeMnNi HEA, and Ni were 2.1×10^{22} , 9.6×10^{21} , 7.0×10^{21} , and 4.0×10^{19} /m³, respectively. Therefore, the density of defects formed by irradiation in the MEAs and HEA was more than two orders of magnitude higher than that in Ni.

In general, because the migration energy of interstitials is lower than that of vacancies in metals and alloys, interstitials preferentially escape to the surface in the shallow part of a thin-film sample in the case of irradiation using thin-film samples. This results in a greater number of vacancies than interstitials, which facilitates the formation of vacancy-type defect clusters in the shallow part of the thin-film sample. Fig. 4 shows dark-field images of the microstructures in the thin parts of the samples shown in Fig. 3. The average thickness of each sample was 60 nm. The microstructures within the blue square (in color figure), which are magnified twice to identify the defects, are inserted into the MEA and HEA photographs. In contrast

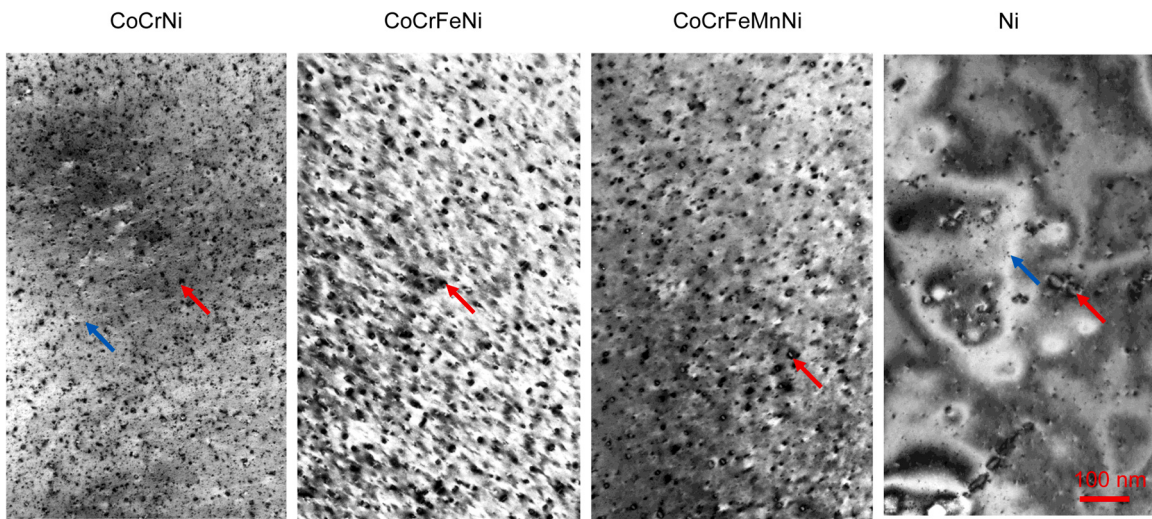


Fig. 3. Bright-field images of microstructures in thin-film CoCrNi and CoCrFeNi MEAs, CoCrFeMnNi HEA, and Ni after ion irradiation at 673 K. The average thickness and damage in the observation area were 130 nm and 1 dpa, respectively. Large and small defect clusters are marked with red and blue arrows, respectively.

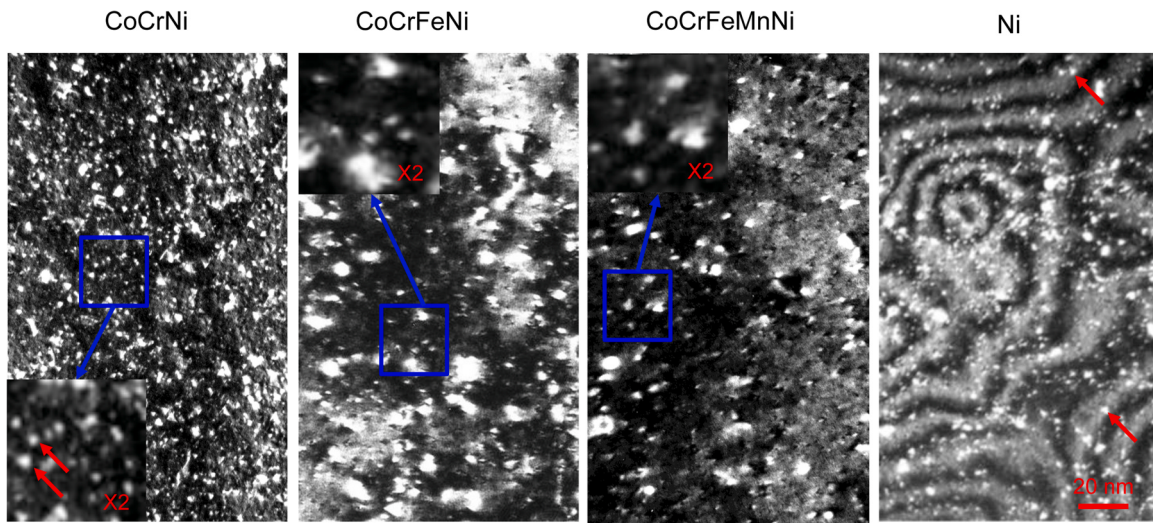


Fig. 4. Dark-field images of microstructures in thin-film CoCrNi and CoCrFeNi MEAs, CoCrFeMnNi HEA, and Ni after ion irradiation at 673 K. The average thickness and damage in the observation area were 60 nm and 1 dpa, respectively. The microstructures within the blue square (in color figure), which are magnified twice, are inserted into the MEAs and HEA photographs. The SFTs are marked with red arrows.

to Fig. 3, the white dots in Fig. 4 represent defects. Similar to Fig. 3, there were two types of defects with large and small sizes in the irradiated samples. Some of the small defects (marked in red) with triangular shapes in the magnified regions of the CoCrNi MEA and Ni were stacking fault tetrahedra (SFTs). However, even in the magnified regions of the CoCrFeNi MEA and HEA, there were no small defects with triangular shapes. The densities of defects induced by irradiation in the shallow parts of the CoCrNi and CoCrFeNi MEA, CoCrFeMnNi HEA, and Ni thin-film samples were 6.7×10^{23} , 1.8×10^{23} , 1.3×10^{23} , and $4.2 \times 10^{23} / \text{m}^3$, respectively. The defect densities in the shallow parts were higher than those in the thick parts. This is because the formation of defect clusters was reduced by the recombination and disappearance of interstitials and vacancies in the thick parts. A similar phenomenon was reported by Kiritani et al. [31,32]. In addition, comparing the thick parts of the samples, the defect density in the CoCrNi MEA was 1.6 times higher than that in Ni, while those in the CoCrFeNi MEA and CoCrFeMnNi HEA were lower.

3.2. Damaged microstructures induced by ion irradiation at high temperature of 873 K

Fig. 5 shows bright-field images of the microstructures in the CoCrNi and CoCrFeNi MEA, CoCrFeMnNi HEA, and Ni thin films after ion irradiation at 873 K. The ion irradiation fluence and thickness of the observation site were the same as those in Fig. 3. After irradiation, voids with sizes of 200 – 300 nm formed in Ni. In contrast, no void formation was observed in the MEAs and HEA. These results suggest that it was difficult to form voids in the MEAs and HEA. Instead of forming voids, precipitates were formed in the CoCrNi and CoCrFeNi MEAs, and dislocation loops were formed in the CoCrFeMnNi HEA. Their densities were 1.6×10^{21} , 2.1×10^{21} , and $3.6 \times 10^{21} / \text{m}^3$ in the CoCrNi and CoCrFeNi MEAs and CoCrFeMnNi HEA, respectively. Fig. 6 shows a stereograph of the precipitates formed in the CoCrNi MEA in thicker areas (~150 nm), and Fig. 7 shows the size distribution of the precipitates. The precipitates extended along the $<110>$ direction. In addition, there were also precipitates in the

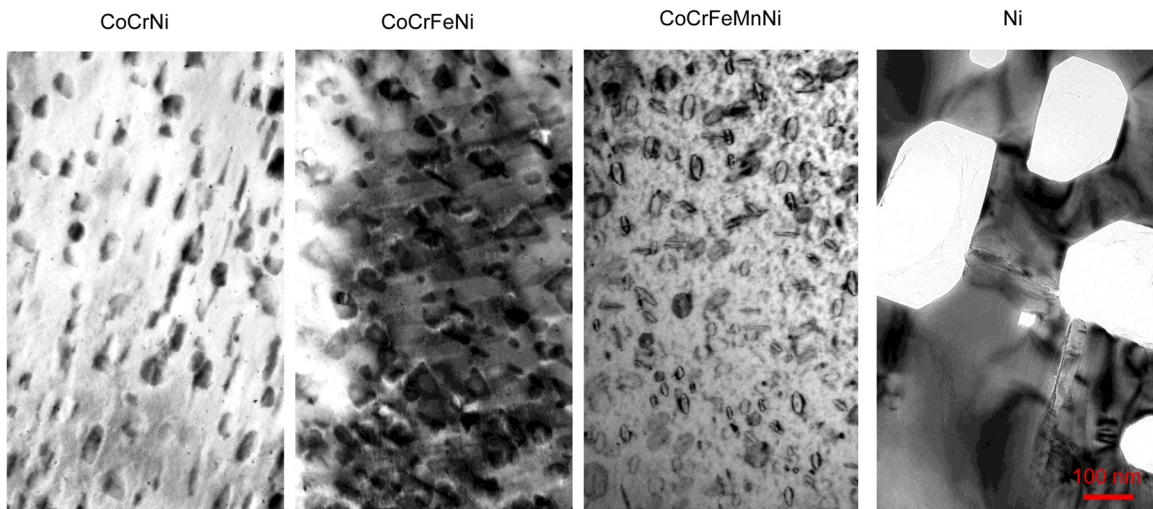


Fig. 5. Bright-field images of microstructures in thin-film CoCrNi and CoCrFeNi MEAs, CoCrFeMnNi HEA, and Ni after ion irradiation at 873 K. The average thickness and damage in the observation area were 130 nm and 1 dpa, respectively.

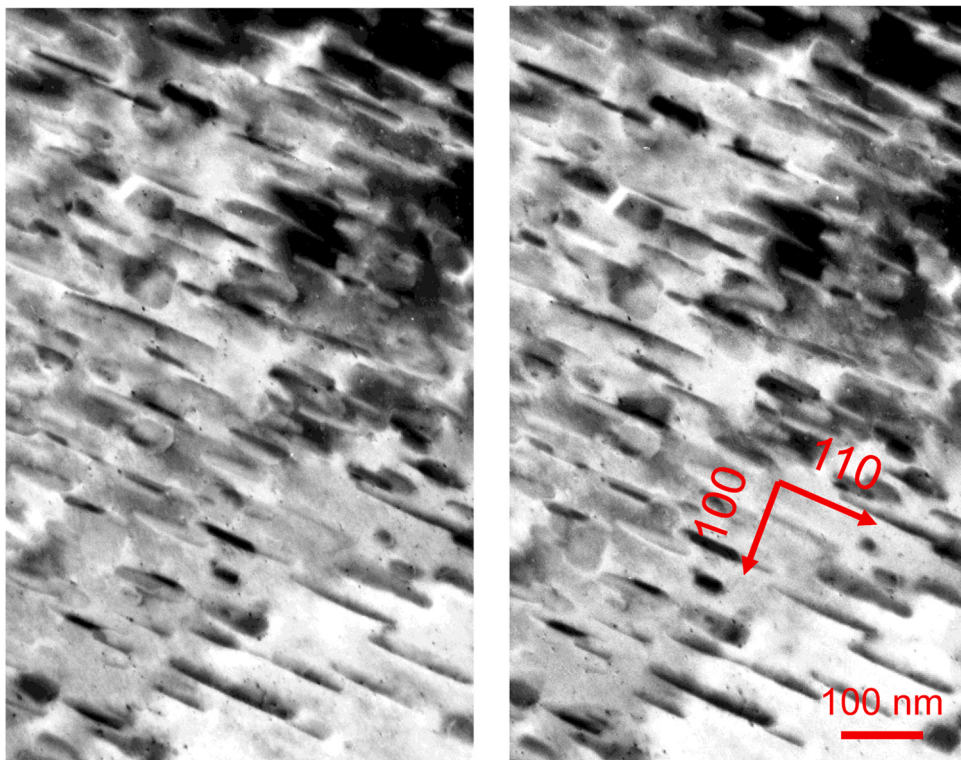


Fig. 6. Stereograph of microstructures in CoCrNi MEA irradiated at 873 K, in which the average thickness and damage in the observation area were 130 nm and 1 dpa, respectively.

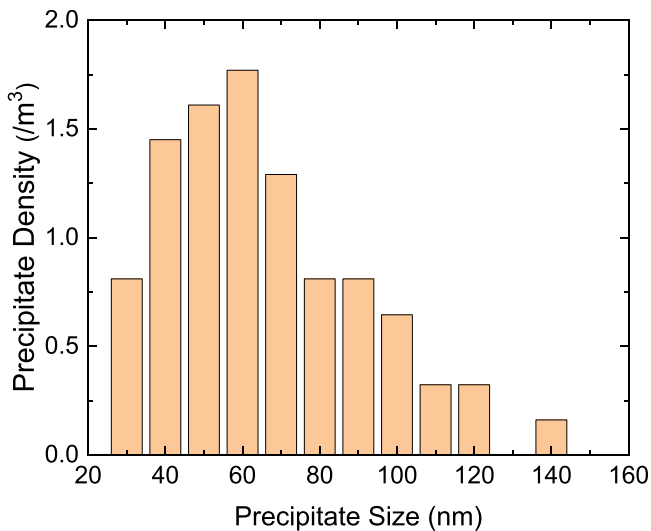


Fig. 7. Size distribution of precipitates in the CoCrNi MEA irradiated at 873 K.

middle of the thin-film sample, although most of the precipitates were concentrated near both surfaces of the sample, at which the concentration of vacancies was higher than that of interstitials. This result suggests that the presence of excess vacancies promotes precipitate formation. EDS analysis was performed to examine the composition of the precipitates. Fig. 8 shows the STEM-EDS map of the irradiated CoCrNi MEA. It is clear that the precipitates induced by irradiation were due to Cr segregation and Co and Fe deficiencies. Similarly, the changes in sample composition due to irradiation in the CoCrFeNi MEA and CoCrFeMnNi HEA were also investigated using EDS analysis. The results are shown in Figs. 9 and 10. Similar to the CoCrNi MEA, Cr segregation and Co, Fe, and Ni deficiencies were observed in the CoCrFeNi MEA after irradiation (Fig. 9). In contrast, in the CoCrFeMnNi HEA (Fig. 10), no segregation or element deficiency due to irradiation was observed.

Similar to Fig. 4, Fig. 11 shows dark-field images of the damaged microstructure in the shallow parts of the thin-film samples due to irradiation at 873 K. Numerous SFTs were formed in the CoCrNi and CoCrFeNi MEAs after irradiation. In contrast, no SFT formation was observed in the CoCrFeMnNi HEA. This result suggests that it was more difficult to form vacancy clusters in the CoCrFeMnNi HEA than in the CoCrNi and CoCrFeNi MEAs. This is consistent with the

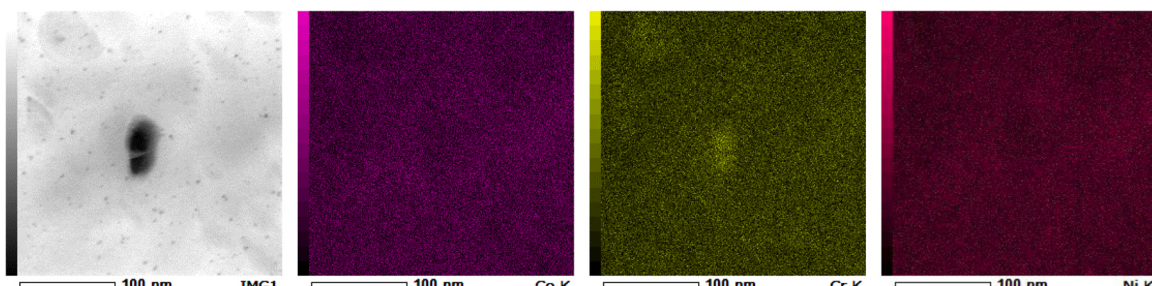


Fig. 8. STEM-EDS map of CoCrNi MEA irradiated at 873 K.

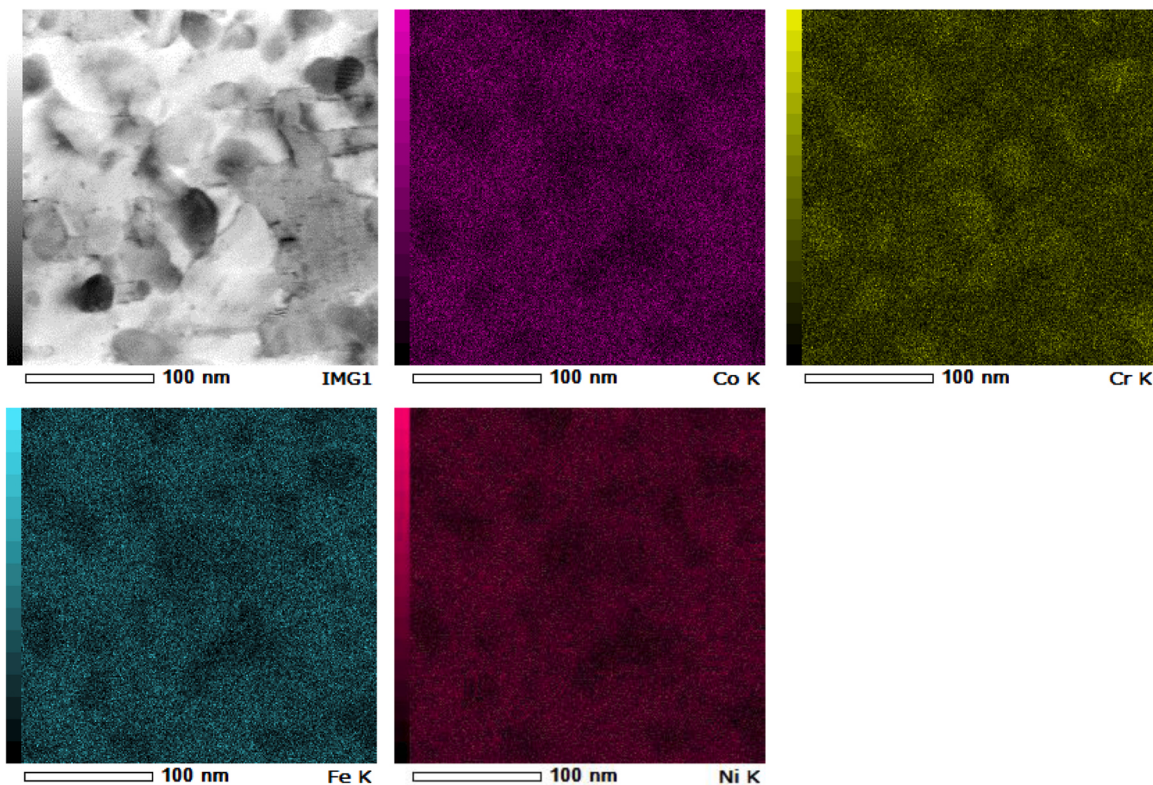


Fig. 9. STEM-EDS map of CoCrFeNi MEA irradiated at 873 K.

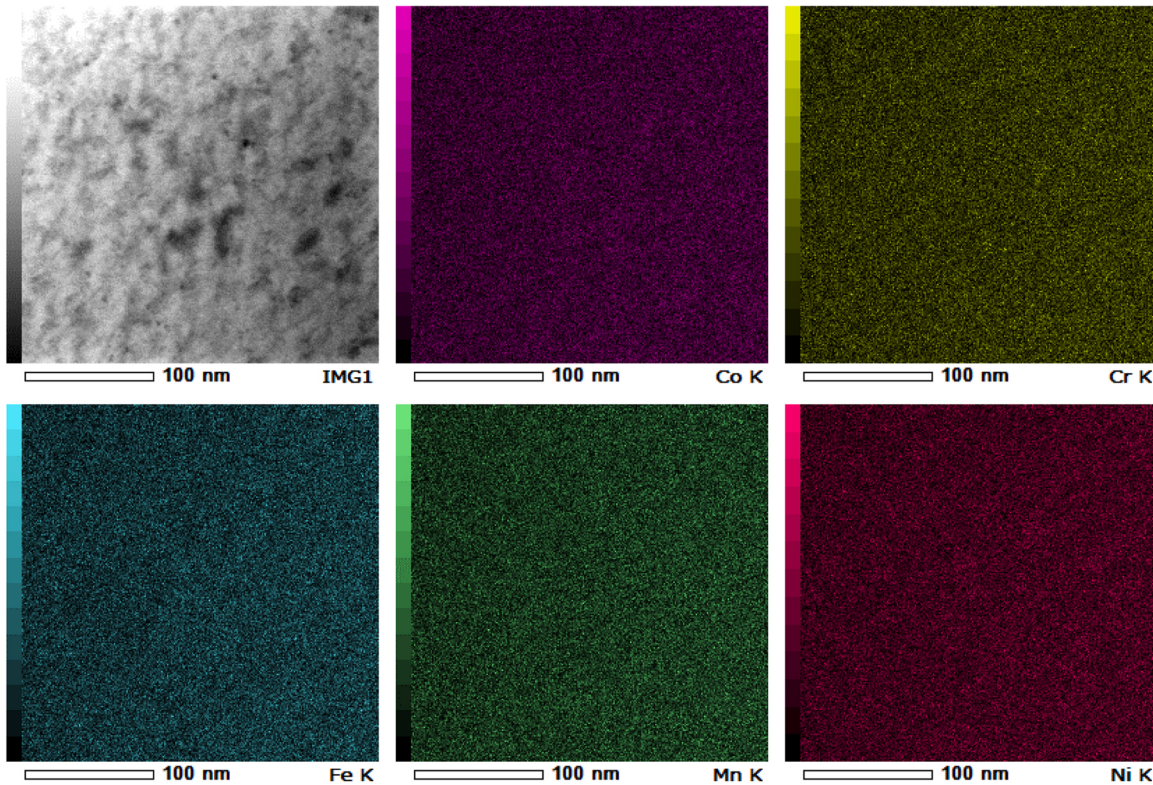


Fig. 10. STEM-EDS map of CoCrFeMnNi HEA irradiated at 873 K.

findings of Xu et al. [32]. The defect densities were 1.7×10^{23} , 1.4×10^{23} , and $5.2 \times 10^{22} / \text{m}^3$ in the CoCrNi and CoCrFeNi MEAs and CoCrFeMnNi HEA, respectively. The defects formed by irradiation in the CoCrFeMnNi HEA are considered to be dislocation loops.

The results of the present experiments show that the defect densities in the CoCrNi and CoCrFeNi MEAs and CoCrFeMnNi HEA were higher than those in Ni under irradiation at low temperatures. Although there is no detailed data on the migration energies of

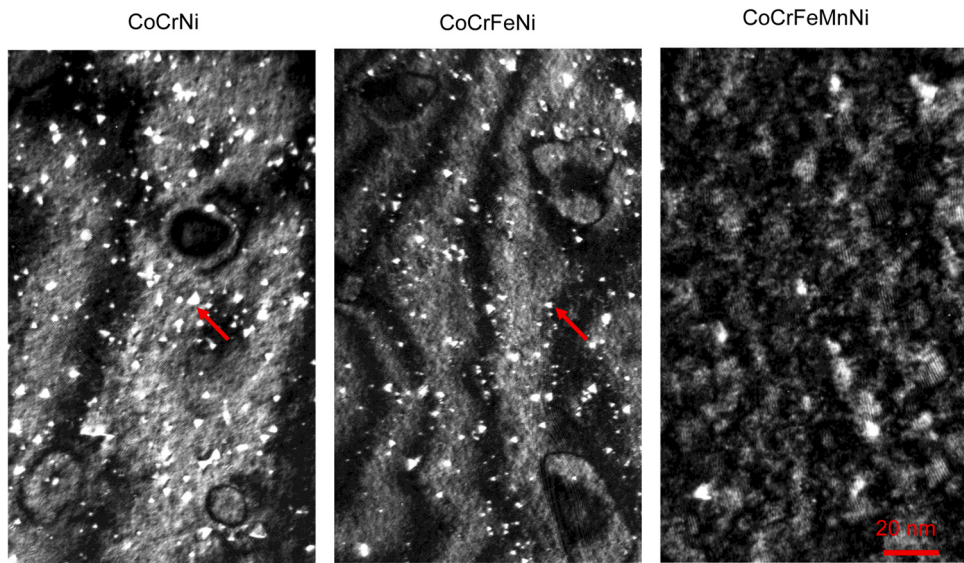


Fig. 11. Dark-field images of microstructures in thin-film CoCrNi and CoCrFeNi MEAs and CoCrFeMnNi HEA after ion irradiation at 873 K. The average thickness and damage in the observation area were 60 nm and 1 dpa, respectively. The SFT is marked with red arrow.

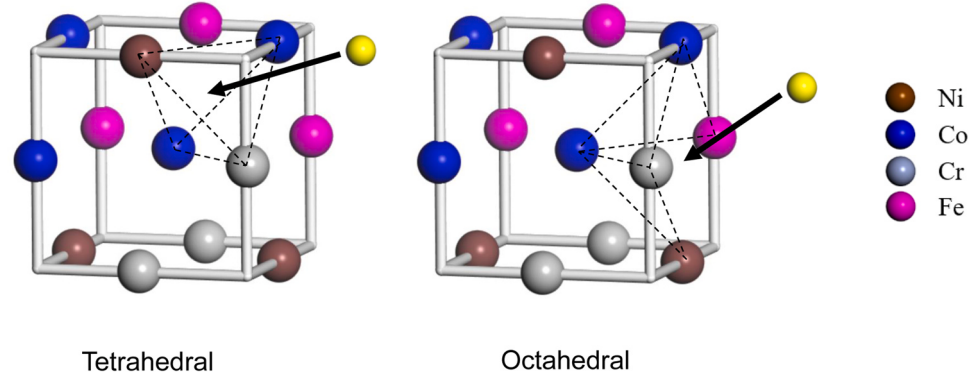


Fig. 12. Schematic figure showing the interstitial positions in CoCrFeNi MEA. The self-interstitial (yellow) is inserted at a tetrahedral (left) and octahedral (right) interstitial position.

interstitials in CoCrNi and CoCrFeNi MEAs and CoCrFeMnNi HEA, the higher defect densities in the MEAs and HEA is hypothesized to be the reason for the higher interstitial migration energies in these alloys compared to that of Ni. Slow-migrating interstitials promote nucleation and prevent interstitial cluster growth. In addition, under irradiation at high temperatures, both the CoCrNi and CoCrFeNi MEAs and CoCrFeMnNi HEA exhibited better irradiation resistance than Ni. In particular, the HEA has a low probability of forming vacancies when irradiated at high temperatures. Xu et al. investigated the SFT formation in CoCrNi and CoCrFeNi MEAs and the CoCrFeMnNi HEA [8,32], and reported that the binding energies of the di-, tri-, and tetra-vacancy clusters in both MEAs were positive, implying that these vacancy clusters were stable. However, the binding energy of the tri-vacancy cluster in the CoCrFeMnNi HEA was negative [8]. Because the tri-vacancy clusters were unstable in the CoCrFeMnNi HEA, the existence of vacancy clusters larger than the tri-vacancy clusters was not likely. Certainly, in the case of neutron and ion irradiations, cascade damage directly forms the vacancy clusters containing four or more vacancies, and these clusters absorb vacancies to form voids [8]. Jin et al. reported the void formation in ion-irradiated CoCrFeMnNi HEA [10]. In addition, the binding energy of the vacancy clusters in Ni increased with the cluster size [8], but did not depend on the sizes of the vacancy clusters in the MEAs and HEA. Even with these results, it was

difficult to explain why the MEAs have better irradiation resistance than Ni. In MEAs and HEA, the irradiation-induced migration barrier of point defects, particularly interstitials, is considered to increase because of the atomic-level stresses caused by atomic size difference. Consequently, the probability of recombination between interstitials and vacancies increases, and the vacancy concentration in MEAs and the HEA decreases. Further research is required on the irradiation resistance of MEAs and the HEA. The present experimental results show that the HEA has a more stable composition even when it is irradiated at high temperature. Although precipitation and segregation may occur easily when CoCrNi and CoCrFeNi MEAs are irradiated under thin film conditions, that is, under a state of excessive vacancies, precipitation and segregation are still likely to occur even in bulk samples if the irradiation fluence is increased.

3.3. Stable state of different element interstitials in CoCrNi and CoCrFeNi MEAs and CoCrFeMnNi HEA

The stable interstitial site in alloys and metals with the FCC structure is located in the middle of a tetrahedron or octahedron. We investigated the interstitial sites in CoCrNi and CoCrFeNi MEAs and CoCrFeMnNi HEA and found that the interstitials at the tetrahedral interstitial sites are more stable. Fig. 12 shows a schematic of the interstitial sites in CoCrFeNi MEA as an example. The self-

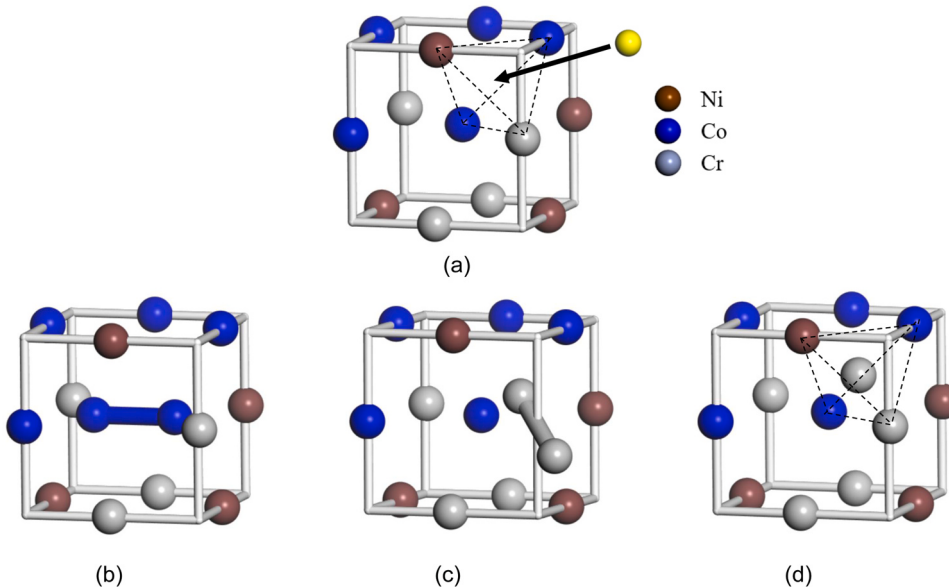


Fig. 13. Stable stage of a self-interstitial in CoCrNi MEA. (a) A self-interstitial is inserted in a tetrahedral interstitial site. (b) Inserted atom interacts with its neighbor to form a dumbbell interstitial along the $<100>$ direction. (c) Inserted atom interacts with its neighbor to form a dumbbell interstitial along the $<111>$ direction. (d) The self-interstitial does not bond with neighbors and is stable at the tetrahedral interstitial site.

interstitials (yellow) are inserted at the tetrahedral (left) and octahedral (right) interstitial sites. According to Eq. (2), the interstitial formation energy at a tetrahedral interstitial site is 3.06 eV, whereas that at an octahedral interstitial site is 4.17 eV. Therefore, the interstitials in the MEAs and HEA occupy tetrahedral rather than octahedral interstitial sites.

Because segregations and precipitations consist of aggregation of solution atoms, it is necessary to investigate the stable interstitial positions for different elements in CoCrNi and CoCrFeNi MEAs and CoCrFeMnNi HEA. In the present study, a self-interstitial was introduced by inserting an interstitial atom into the tetrahedral interstitial site. As an example, Fig. 13 (a) shows the introduction of a self-interstitial into CoCrNi MEA. Because of the large numbers of tetrahedral interstitial sites and self-interstitials with different elements in the CoCrNi and CoCrFeNi MEAs and CoCrFeMnNi HEA, more than tens of cases were investigated to perform a statistical analysis of the influence of the local environment on the interstitial formation energy. As shown in Fig. 13 (b) – (d), when a self-interstitial is inserted in a tetrahedral interstitial site (Fig. 13 (a)), three types of stable states may result. In the first type, the inserted atom interacts with its neighbor to form a dumbbell interstitial along the $<100>$ direction (Fig. 13 (b)). In the second type, the inserted atom interacts with its neighbor to form a dumbbell interstitial along the $<111>$ direction (Fig. 13 (c)). In the third type, the self-interstitial does not bond with its neighbors and is stable at the tetrahedral interstitial site (Fig. 13 (d)). There is another important but low-probability case in which a dumbbell interstitial, such as that shown in Fig. 13 (b) and (c), or a stable interstitial at the tetrahedral interstitial site (Fig. 13 (d)) is not formed by the inserted interstitial but, rather, by an atom that previously formed the tetrahedron and has now replaced the inserted interstitial. Table 1 lists the average values of the stable interstitial formation energies at the tetrahedral interstitial site of CoCrNi MEA. The numbers of calculations are listed in the table. When Co occupied the tetrahedral interstitial site, the formation probability of a Co dumbbell was almost 100 %, which is consistent with the fact that dumbbells are often the most stable interstitials in alloys [25]. Among such dumbbells, Co-Co and Co-Cr dumbbells along the $<100>$ direction each accounted for 40 % of the formation probability, and Co-Cr dumbbells along the $<111>$ direction the remaining 20 %. However, when Cr occupied

the tetrahedral interstitial site, only Cr-Cr dumbbells along the $<111>$ direction and stable Cr interstitials were formed with the formation probabilities of 30 % and 70%, respectively. In contrast, when Ni occupied the tetrahedral interstitial site, in addition to Ni-Cr and Ni-Co dumbbells along the $<100>$ direction, Co-Co and Co-Cr dumbbells along the $<100>$ direction with no inserted Ni were also formed through the displacement of Co constituting the tetrahedron by Ni at the tetrahedral site. Although the higher formation energy of Cr interstitials (3.48 eV) compared to Co (3.15 eV) and Ni (3.07 eV) interstitials (lower part of Table 1) implies that Cr interstitials were less easily formed than Co or Ni interstitials, the probability of Cr-dumbbell formation was higher than those of Ni- and Co-dumbbells. Most Cr interstitials formed Cr-Cr dumbbells (approximately 30 %) or remained by themselves (70 %). These Cr interstitials could move to the Cr dumbbells and precipitate. Co interstitials formed Co-Co dumbbells (40 %) in addition to Co-Cr dumbbells (60 %). There were only a few stable Co interstitials. Compared with Cr and Co interstitials, there was a lower rate of dumbbell formation between Ni interstitials and Cr (40 %). Moreover, the Ni-occupying the tetrahedral interstitial site pushed out the Co that made up the tetrahedron. This Co then occupied the tetrahedral interstitial site of the adjacent tetrahedron (this process is labeled as Ni-Co in Table 1) and formed a dumbbell with Co or Cr. Considering this process, the probability of direct or indirect dumbbell formation between Ni interstitials and Cr was 60 %, which is the same as the Co-Cr dumbbell formation probability. Therefore, these calculation results suggest that the probability of Cr segregation in CoCrNi MEA is much higher than that of Co and Ni segregation.

Table 2 lists the average values of the stable interstitial formation energies in the tetrahedral interstitial site of CoCrFeNi MEA in correspondence to what was shown for CoCrNi in Table 1. In CoCrFeNi MEA, as in CoCrNi MEA, dumbbells were formed easily after one atom of different elements was inserted at the tetrahedral interstitial site. When Co occupied the tetrahedral interstitial site, the probability of Co-Cr dumbbell formation (40 %) was higher than those of other Co-dumbbells. When Cr occupied the tetrahedral interstitial site, Cr-Fe and Cr-Co dumbbells could be formed in addition to Cr-Cr dumbbells but with a lower probability (20 %). The formation probabilities of Cr-Cr dumbbells were 50% and that of stable Cr

Table 1

Average values of stable interstitial formation energies and numbers of calculations for CoCrNi MEA.

Co			Cr			Ni		
Configuration	Number of calculations	Mean value (eV)	Configuration	Number of calculations	Mean value (eV)	Configuration	Number of calculations	Mean value (eV)
< 100 > Co-Co	4	3.13	< 111 > Cr-Cr	3	3.48	< 100 > Ni-Cr	4	3.12
< 100 > Co-Cr	4	3.02	Cr	7	3.48	< 100 > Ni-Co	3	3.31
< 111 > Co-Cr	2	3.45				Ni → Co	1	2.94
Average Energy (eV)			Co	3.15	Cr	3.48	Ni → Co	2
						< 100 > Co-Cr		2.67
						Ni	3.07	

interstitials 30 %, which is lower compared to the formation probability in CoCrNi MEA. The probability of forming Cr-related dumbbells was 70 % when Fe occupied the tetrahedral interstitial site. When Ni occupied the tetrahedral interstitial site, the probability of forming Cr dumbbells directly or indirectly was 50 %. In addition, the probability of forming stable Cr interstitials was 10%. Compared to CoCrNi MEA, the formation probability of dumbbells with Cr or stable Cr interstitials in CoCrFeNi MEA was slightly lower, but still much higher than the proportion of each element (25 %). The average value of the Cr interstitial formation energy (3.5 eV) is higher than those of the other elements.

Table 3 lists the average values of the stable interstitial formation energies in the tetrahedral interstitial site of CoCrFeMnNi HEA. Because there were more types of dumbbells in CoCrFeMnNi HEA, the proportion of Cr-dumbbells decreased. As listed in Table 3, when Co occupied the tetrahedral interstitial site, the probability of forming Co-Cr dumbbells was 20 %. Conversely, the probability of forming Mn-dumbbells, either directly or indirectly, was 40 %. When Cr occupied the tetrahedral interstitial site, the formation probabilities of Cr-Cr dumbbells along the < 111 > direction and stable Cr interstitials decreased further to 40 % and 20 %, respectively. When Fe occupied the tetrahedral interstitial site, the formation probabilities of Cr- and Mn-dumbbells (directly or indirectly) were the same at 40 %. When Mn occupied the tetrahedral interstitial site, the formation probabilities of Mn-Mn dumbbells along the < 111 > direction and stable Mn interstitials decreased further to 40 % and 20 %, respectively. The latter was the same probability as that of Cr self-interstitials. In addition, the probability of indirectly forming Cr-

dumbbells was 20 %. When Ni occupied the tetrahedral interstitial site, the probability of forming Cr-dumbbells directly or indirectly decreased to 40 %; however, the probability of forming Mn-dumbbells directly or indirectly remained unchanged. In CoCrFeMnNi HEA, the formation probability of Cr-dumbbells was slightly higher than that of Mn-dumbbells. However, because there were equal probabilities for stable Cr and Mn interstitials to be formed, the segregation of Cr by itself in the HEA due to irradiation was unremarkable. In addition, as with the CoCrNi and CoCrFeNi MEAs, the average value of the Cr interstitial formation energy (3.55 eV) was higher than those of the other elements.

The first-principles calculation results in the present study indicate that the probability of Cr segregation is higher in CoCrNi and CoCrFeNi MEAs than in CoCrFeMnNi HEA, which is in good agreement with the experimental results. In the CoCrNi MEA, 60% of the Co and Ni interstitials form Cr-dumbbells directly or indirectly, whereas Cr interstitials either form Cr-Cr dumbbells (30%) or remain unchanged (70%). The preferential formation of Cr-dumbbells and the free migration of Cr interstitials contributes to Cr segregation during irradiation. In CoCrFeNi MEA, which has one more element than CoCrNi MEA, the formation probabilities of both Cr-dumbbells and stable Cr interstitials (30%) are reduced. This decreases Cr segregation during irradiation. In CoCrFeMnNi HEA, the probability of forming Cr-dumbbells and stable Cr interstitials (20%) is further reduced, while the probability of Mn-dumbbell and stable Mn interstitial formation is increased, and becomes the same as that of Cr-dumbbell and stable Cr interstitial formation. Therefore, Cr segregation during irradiation is eliminated. These calculations do not

Table 2

Average values of stable interstitial formation energies and numbers of calculations for CoCrFeNi MEA.

Inserted			self-interstitial								
Co			Cr			Fe			Ni		
Conf.	Cals.	E (eV)	Conf.	Cals.	E (eV)	Conf.	Cals.	E (eV)	Conf.	Cals.	E (eV)
< 100 > Co-Fe	3	3.15	< 111 > Cr-Cr	4	3.43	< 111 > Fe-Cr	3	3.13	< 100 > Ni-Cr	4	2.86
< 100 > Co-Co	1	2.61	< 110 > Cr-Cr	1	3.27	< 100 > Fe-Cr	2	2.37	< 100 > Ni-Fe	2	2.9
< 100 > Co-Cr	3	2.99	< 111 >	1	3.74	< 100 > Fe-Fe	1	3.11	< 100 > Ni-Co	1	3.05
< 111 > Co-Cr	1	2.9	Cr-Fe			Fe → Co	1	2.66	Ni → Fe	1	2.43
			< 111 >	1	3.2	< 100 >			< 100 >		
			Cr-Co			Co-Cr			Fe-Fe		
Co → Fe	1	2.81	Cr	3	3.7	Fe → Cr	1	2.83	Ni → Co	1	2.5
< 100 >			< 111 >			< 111 >			< 100 >		
Fe-Fe			Cr-Cr			Cr-Cr			Co-Cr		
Co → Fe	1	2.98	Fe	2	3.68	Fe	2	3.68	Ni → Cr	1	2.98
< 100 >									Cr		
Fe-Co											
Average Energy (eV)			Co	2.97	Cr	3.5	Fe	3.01	Ni	2.82	

Table 3
Average values of stable interstitial formation energies and numbers of calculations for CoCrFeMnNi HEA.

Co	Inserted self-interstitial						Ni	
	Cr	Fe	Mn	Ni	Cals.	E (eV)		
Conf.	Cals.	E (eV)	Conf.	Cals.	E (eV)	Conf.	Cals.	E (eV)
< 100 > Co-Fe	1	2.67	< 111 > Cr-Cr	2	3.47	< 111 > Fe-Mn	1	2.89
< 100 > Co-Mn	1	2.25	< 111 > Cr-Co	1	3.59	< 100 > Fe-Fe	1	2.91
< 100 > Co-Cr	1	2.43	< 111 > Cr-Fe	1	3.7	Re → Co	2	2.4
Co → Ni	1	2.56	Cr	1	3.51	< 100 > Co-Cr		
< 100 > Ni-Mn						Fe → Ni	1	2.95
Co → Cr	1	2.4				Fe → Ni	1	2.95
< 111 > Cr-Mn						< 100 > Ni-Mn		
Average Energy (eV)		2.46	Co	2.46	3.55	Cr	3.55	2.71
						Fe	2.71	2.97
						Mn	2.97	2.71
						Ni	2.71	

consider the relationship between Cr precipitate formation and the irradiation temperature, and the growth of Cr precipitates. Further research is required to address these issues.

To elucidate the mechanisms behind the irradiation resistance and excellent mechanical properties of CoCrNi and CoCrFeNi MEAs and CoCrFeMnNi HEA, the short-range ordering (SRO) in these alloys has been studied through both experiments and calculations [33–37]. Inoue et al. investigated the spatial distribution of elements in CoCrNi MEA using atom probe tomography (APT) and found that the distribution of Co, Cr, and Ni was non-uniform, particularly in a sample annealed at 973 K for 384 h, in which Cr-rich {001} and (Ni + Co)-rich {001} atomic layers tended to align mutually inside a region of 10 at. distances (~2 nm) [35]. This result suggests that the composition of CoCrNi MEA is not uniform and its components may segregate, which is in agreement with the results of the present ion-irradiation experiment and calculations. Ren et al. reported that the elemental distribution in CoCrFeMnNi HEA is disordered, despite the favorable affinity between Cr and Ni according to calculation results [37], which is in agreement with the present experiment and calculation results. In the present study, segregation due to irradiation was observed in the CoCrNi and CoCrFeNi MEA thin-film samples. However, similar irradiation experiments will need to be performed on bulk samples in the future to confirm segregation.

4. Conclusion

Because the stability of an alloy composition affects its irradiation resistance, the composition changes due to the irradiation of CoCrNi and CoCrFeNi MEAs and CoCrFeMnNi HEA were investigated in this study. The irradiation resistance of these alloys was compared to that of Ni.

The thin-film samples of CoCrNi and CoCrFeNi MEAs, CoCrFeMnNi HEA, and Ni were irradiated with up to 1.7×10^{19} ions/ m^2 of 2.4 MeV Cu ions at 673 and 873 K and the resultant microstructure and composition analyzed. At 673 K, interstitial dislocation loops were formed in all the samples. However, the formation of SFTs in the CoCrNi and CoCrFeNi MEAs and CoCrFeMnNi HEA was suppressed compared to Ni, in which there was significant formation of SFTs. In addition, the density of defects formed by irradiation in the MEAs and HEA was more than two orders of magnitude higher than that in Ni. At 873 K, voids were formed in Ni, whereas no void formation was observed in the MEAs and HEA. Therefore, the irradiation resistance of the MEAs and HEA was superior to that of Ni. In addition, Cr segregation due to irradiation was observed in the MEAs, whereas no Cr segregation was observed in the HEA.

The segregation behavior of the elements in CoCrNi and CoCrFeNi MEAs and CoCrFeMnNi HEA was investigated using the first-principles calculations. In CoCrNi and CoCrFeNi MEAs, the formation of Cr-dumbbell with elements other than Cr had the highest probability. Cr interstitials formed only Cr-Cr dumbbells or remained as stable interstitials. This tendency promoted the Cr segregation under irradiation. In addition, the probability of stable Cr interstitial formation in CoCrFeNi was lower than that in CoCrNi MEA. In comparison, in CoCrFeMnNi HEA, the probabilities of forming Cr-dumbbells and stable Cr interstitials decreased and the probabilities of forming Mn-dumbbells and stable Mn interstitials increased to the same levels as those of Cr. Therefore, the Cr segregation during irradiation was no longer remarkable.

CRediT authorship contribution statement

Q. X: Writing, Investigation, Supervision and Conceptualization, Writing - original draft, Writing - review & editing. **H. G:** Data curation. **S. H:** Data curation. **Z. Z:** Investigation, Data curation. **H. W:** Data curation. **M. T:** Data curation.

Data Availability

No data was used for the research described in the article.

Declaration of Competing Interest

The authors declare that they have no known competing financial interests or personal relationships that could have appeared to influence the work reported in this paper.

References

- [1] B. Cantor, I.T.H. Chang, P. Knight, A.J.B. Vincent, Microstructural development in equiatomic multicomponent alloys, *Mater. Sci. Eng. A* 375–377 (2004) 213–218.
- [2] D.B. Miracle, J.D. Miller, O.N. Senkov, C. Woodward, M.D. Uchic, J. Tiley, Exploration and development of high entropy alloys for structural applications, *Entropy* 16 (2014) 494–525.
- [3] F. Otto, Y. Yang, H. Bei, E.P. George, Relative effects of enthalpy and entropy on the phase stability of equiatomic high-entropy alloys, *Acta Mater.* 61 (2013) 2628–2638.
- [4] B. Gludovatz, E.P. George, R.O. Ritchie, Processing, microstructure and mechanical properties of the CrMnFeCoNi high-entropy alloy, *JOM* 67 (2015) 2262–2270.
- [5] E.J. Pickering, N.G. Jones, High-entropy alloys: a critical assessment of their founding principles and future prospects, *Int. Mater. Rev.* 61 (2016) 183–202.
- [6] E.P. George, D. Raabe, R.O. Ritchie, High-entropy alloys, *Nat. Rev. Mater.* 4 (2019) 515–524.
- [7] X.L. Ren, Z.H. Zhong, T. Zhu, B.D. Yao, Y.X. Wang, X.Z. Cao, S. Jinno, Q. Xu, Effect of irradiation on randomness of element distribution in CoCrFeMnNi equiatomic high-entropy alloy, *Intermetallics* 126 (2020) 106942.
- [8] Q. Xu, H.Q. Guan, Z.H. Zhong, S.S. Huang, J.J. Zhao, Irradiation resistance mechanism of the CoCrFeMnNi equiatomic high-entropy alloy, *Sci. Rep.* 11 (2021) 608.
- [9] Y.E. Li, R. Li, Q. Peng, Enhanced surface bombardment resistance of the CoNiCrFeMn high entropy alloy under extreme irradiation flux, *Nanotechnology* 31 (2020) 025703.
- [10] K. Jin, C. Lu, L.M. Wang, J. Qu, W.J. Weber, Y. Zhang, H. Bei, Effects of compositional complexity on the ion-irradiation induced swelling and hardening in Ni-containing equiatomic alloys, *Scr. Mater.* 119 (2016) 65–70.
- [11] L.X. Yang, H.L. Ge, J. Zhang, T. Xiong, Q.Q. Jin, Y.T. Zhou, X.H. Shao, B. Zhang, Z.W. Zhu, S.J. Cheng, X.L. Ma, High He-ion irradiation resistance of CrMnFeCoNi high-entropy alloy revealed by comparison study with Ni and 303SS, *J. Mater. Sci. Technol.* 35 (2019) 300–305.
- [12] Q. Xu, Z.H. Zhong, to be published.
- [13] A. Gali, E.P. George, Tensile properties of high- and medium-entropy alloys, *Intermetallics* 39 (2013) 74–78.
- [14] C.Y. Lu, T.N. Yang, K. Jin, G. Velisa, P.Y. Xiu, Q. Peng, F. Gao, Y.W. Zhang, H.B. Bei, W. Weber, L.M. Wang, Irradiation effects of medium-entropy alloy NiCoCr with and without pre-indentation, *J. Nucl. Mater.* 524 (2019) 60–66.
- [15] M. Kiritani, T. Yoshiie, S. Kojima, Y. Satoh, K. Hamada, Fission fusion correlation by fission reactor irradiation with improved control, *J. Nucl. Mater.* 174 (1990) 327–351.
- [16] M. Kiritani, Y. Fukuta, T. Mima, E. Iiyoshi, Y. Kizuka, S. Kojima, N. Matsunani, Form. Vacancy Clust. Eff. cascade Collis. Heavy-Ion-. Irradiat. their Annihil. Free.-migrating Inter., *J. Nucl. Mater.*, 212–251, 1994, pp. 192–197.
- [17] T. Yoshiie, M. Kiritani, Eff. cascade Local. Induc. bias Eff. Fluct. Point Defect React. Defect Struct. Evol. Planar Sinks, *J. Nucl. Mater.* 212–215 1994 315 319.
- [18] Q. Xu, H. Watanabe, T. Muroga, N. Yoshida, Effects of temperature variation on damage microstructures in Fe-Cr-Ni alloy induced by heavy ion irradiation, *J. Nucl. Mater.* 212–251 (1994) 258–262.
- [19] Ziegler J. SRIM-2008, v.2008.40 (2008). Available at <<http://www.srim.org>>.
- [20] A.V. Kozlov, V.V. Kirsanov, Radiation defect formation and evolution in C0.03Cr20Ni16Mn6 steel under low-temperature neutron irradiation and their effect on physical and mechanical properties of the steel, *J. Nucl. Mater.* 233–237 (1996) 1062–1066.
- [21] A. Bourret, Irradiation damage in nickel and iron in a high-voltage electron microscope and threshold energy determination, *Phys. Status Solidi A* 4 (1971) 813–825.
- [22] M. Kiritani, Electron radiation damage of metals and nature of point defects by high voltage electron microscopy, in: M. Doyama, S. Yoshida (Eds.), *Progress in the Study of Point Defects*, University of Tokyo Press, 1977, pp. 247–327.
- [23] P.B. Hirsch, A. Howie, M.J. Whelan, A kinematical theory of diffraction contrast of electron transmission microscope images of dislocations and other defects, *Philos. Trans. R. Soc. A* (1960) 449–529.
- [24] J.W. Edington, Interpretation of transmission electron micrographs, Trademarks of Philips' Gloeilampenfabrieken Press, 1975.
- [25] H.Q. Guan, S.S. Huang, J.H. Ding, F.Y. Tian, Q. Xu, J.J. Zhao, Chemical environment and magnetic moment effects on point defect formations in CoCrNi-based concentrated solid-solution alloys, *Acta Mater.* 187 (2020) 122–134.
- [26] G. Kresse, Ab initio molecular dynamics for liquid metals, *J. Non-Cryst. Solids* 192 (1995) 222–229.
- [27] G. Kresse, J. Hafner, Ab initio molecular-dynamics simulation of the liquid-metal-amorphous-semiconductor transition in germanium, *Phys. Rev. B* 49 (1994) 14251–14269.
- [28] G. Kresse, J. Furthmüller, Efficiency of ab-initio total energy calculations for metals and semiconductors using a plane-wave basis set, *Comput. Mater. Sci.* 6 (1996) 15–50.
- [29] F. Tian, D.Y. Lin, X. Gao, Y.F. Zhao, H.F. Song, A structural modeling approach to solid solutions based on the similar atomic environment, *J. Chem. Phys.* 153 (2020) 034101.
- [30] S.H. Wei, L.G. Ferreira, J.E. Bernard, A. Zunger, Electronic properties of random alloys: special quasirandom structures, *Phys. Rev. B* 42 (1990) 9622–9649.
- [31] M. Kiritani, T. Yoshiie, S. Kojima, Y. Satoh, K. Hamada, Fission-fusion correlation by fission reactor irradiation with improved control, *J. Nucl. Mater.* 174 (1990) 327–351.
- [32] Q. Xu, H.Q. Guan, S.S. Huang, Z.H. Zhong, Comparative study of vacancy cluster formation in pure Ni, CoCrNi, and CoCrFeNi with a CoCrFeMnNi multicomponent system, *J. Alloy. Compd.* 918 (2022) 165747.
- [33] F.X. Zhang, S. Zhao, K. Jin, H. Xue, G. Velisa, H. Bei, R. Huang, J.Y.P. Ko, D.C. Pagan, J.C. Neufeind, W.J. Weber, Y. Zhang, Local structure and short-range order in a NiCoCr solid solution alloy, *Phys. Rev. Lett.* 118 (2017) 205501.
- [34] R. Zhang, S. Zhao, J. Ding, Y. Chong, T. Jia, C. Ophus, M. Asta, R.O. Ritchie, A.M. Minor, Short-range order and its impact on the CrCoNi medium-entropy alloy, *Nature* 581 (2020) 283–287.
- [35] K. Inoue, S. Yoshida, N. Tsuji, Direct observation of local chemical ordering in a few nanometer range in CoCrNi medium-entropy alloy by atom probe tomography and its impact on mechanical properties, *Phys. Rev. Mater.* 5 (2021) 085007.
- [36] Y. Zheng, W. Lu, F. Qian, N. Jia, Y. Dou, X. He, W. Wang, J. Wang, Y. Xue, K. Jin, Self-ion irradiation response of (CoCrFeNi)94Ti2Al4 alloy containing coherent nanoprecipitates, *J. Nucl. Mater.* 549 (2021) 152889.
- [37] X.L. Ren, B.D. Yao, T. Zhu, Z.H. Zhong, Y.X. Wang, X.Z. Cao, S. Jinno, Q. Xu, Effect of irradiation on randomness of element distribution in CoCrFeMnNi equiatomic high-entropy alloy, *Intermetallics* 126 (2020) 106942.